

# Replay-based Recovery for Autonomous Robotic Vehicles from Sensor Deception Attacks

Pritam Dash\*, Guanpeng Li†, Mehdi Karimibiuki\*, Karthik Pattabiraman\*

\*University of British Columbia

{pdash, mkarimib, karthikp}@ece.ubc.ca

†University of Iowa

guanpeng-li@uiowa.edu

**Abstract**—Sensors are crucial for autonomous operation in robotic vehicles (RV). Unfortunately, RV sensors can be compromised by physical attacks such as tampering or spoofing, leading to a crash. In this paper, we present *DeLorean*, a model-free recovery framework for recovering autonomous RVs from sensor deception attacks (SDA). *DeLorean* is designed to recover RVs even from a strong SDA in which the adversary targets multiple heterogeneous sensors simultaneously (even all the sensors). Under SDAs, *DeLorean* inspects the attack induced errors, identifies the targeted sensors, and prevents the erroneous sensor inputs from being used to derive actuator signals. *DeLorean* then replays historic state information in the RV’s feedback control loop for a temporary mitigation and recovers the RV from SDA. Our evaluation on four real and two simulated RVs shows that *DeLorean* can recover RVs from SDAs, and ensure mission success in 90.7% of the cases on average.

## I. INTRODUCTION

Autonomous Robotic Vehicles (RV) such as drones and rovers rely on their on-board sensors to perceive their physical states (e.g., position, angular orientation). Based on the physical states, specialized algorithms plan the RV’s mission trajectory and autonomously navigate it. Unfortunately, attackers can feed erroneous sensor measurements to the RV through its physical channels (i.e., physical attacks), causing the RV to deviate from its course and/or result in a crash [38], [51]. Physical attacks such as GPS spoofing have been mounted against military drones [36] and marine systems [35].

Physical attacks cannot be mitigated by traditional security techniques as they target the sensor hardware rather than the software. Further, attack detection [28], [46] alone is not enough, as the RV may still deviate from its course, or crash even after the detection [30]. Activating fail-safe (e.g., forced landing a drone) after attack detection is not always safe, as the drone may land in adverse environments or may end up falling into the attacker’s hands [7].

Typically, RVs estimate physical states based on sensor measurements, and use PID controllers (Proportional Integral Derivative) for deriving appropriate actuator signals in a feedback control loop. Because a physical attack manipulates the RV’s sensor measurements, the corresponding physical states get corrupted. Therefore, the PID controller derives erroneous actuator signals that result in the RV deviating from its trajectory and/or crashing [30].

Prior work has proposed techniques such as software sensors-based recovery (SSR) [27] and PID-Piper [30] for

recovering RVs from physical attacks. Unfortunately, these recovery techniques are only effective when a single sensor or set of sensors of the same type is under attack, but not when multiple sensors of different types are simultaneously targeted (as we show later in the paper). The feasibility of attacks targeting multiple sensors simultaneously has been demonstrated on bare metal systems [44] and autonomous driving systems [24]. We extend this attack setting to RVs, and demonstrate the impact of attacks that target multiple heterogeneous sensors of RVs. Henceforth, we refer to single and multiple sensor attacks collectively as *Sensor Deception Attacks* (SDA).

A fundamental issue with prior approaches is that they are based on predictive model of the RV’s behavior which is used to derive actuator signals under attack, and hence they always tolerate an error margin (approximation error) between model estimations and the RV’s real behaviour. The error margin is small enough under single sensor attacks to derive robust actuator signals for recovering the RV. However, when multiple sensors are attacked simultaneously, the model’s approximation error increases. Thus, both SSR and PID-Piper are ineffective under multi-sensor attacks.

There are two challenges that a recovery technique must address: 1) Prevent erroneous feedback to the PID controller. 2) Derive actuator signals that safely maneuvers RV under SDAs.

In this paper, we present *DeLorean*, a framework to recover RVs from SDAs. *DeLorean* integrates with existing attack detection techniques [28], [30], [46], and provides attack recovery from SDAs. Unlike prior work, *DeLorean* does not require a predictive model of the RV. *DeLorean* follows a model-free approach, and uses the standard PID controller in RVs for attack recovery. *DeLorean* is based on the observation that because physical attacks are launched using fake signal emitters (e.g., acoustic, magnetic, or fake GPS), the fake signals are confined to a physical range (i.e, attack zone). Beyond this range, the fake signals will not be strong enough to influence the sensors [38], [39], [54]. Furthermore, it is difficult for the attacker to follow the RV’s trajectory and emit fake signals that interfere with the RV’s sensors at their natural frequencies [54] (which is needed for the attack to be successful). Thus, to recover RVs from attacks, it is sufficient to derive actuator signals to safely maneuver the RV out of the attack zone, and recalculate the mission trajectory.

*DeLorean* addresses the above challenges through two innovations. First, it uses a *graph-based probabilistic*

method [23] to reason about abnormalities in the RV's physical states under SDA, identify the sensors targeted by the attack, and isolate those sensors from the RV's feedback control loop. This prevents erroneous feedback to the PID controller (challenge 1). Second, for the sensors identified to be under attack, *DeLorean* replays the historic state information collected from an attack-free phase of the RV mission as substitution inputs to the PID controller in the feedback control loop to derive robust actuator signals under attacks (challenge 2).

By isolating the sensors under attack and replaying the safe historical states to the PID controller, *DeLorean* applies a temporary mitigation that controls the state estimation error regardless of the attack (i.e., state estimation error remains constant or shows steady trends). This prevents uncontrolled fluctuations in the actuator signals under SDAs, thereby allowing the RV to be safely maneuvered out of the attack zone. This approach is inspired by Dead Reckoning [21], a method used for deriving the current position and heading direction using past estimates in aircraft and ships, when sensors are not available (e.g., due to adverse weather conditions).

The main assumption behind replay-based recovery is that the environmental conditions prevailing in the RV right before the attack are likely to be the same even under the attack, and hence, the physical states are likely to be similar as well. This is because the attack is restricted to a physical range (attack zone), and hence the duration of the attack is limited. This is why by replaying the historic states, the PID controller is able to recover safely. However, if there is a drastic change in the environmental conditions at the time of the attack, replay-based recovery will not be as effective.

To the best of our knowledge, *DeLorean* is the first model-free technique recovery technique for to recover RVs from SDAs. Our contributions are:

- Design a graph-based probabilistic approach to reason about abnormalities in the RV's states and identify the sensors targeted by SDAs.
- Propose a model-free approach to recover RVs from SDAs by replaying the sequence of safe historic states in the RV's feedback control loop for sensors targeted by SDAs.
- Design *DeLorean*, an automated framework that integrates with existing attack detection techniques for RVs, and provides both attack diagnosis and recovery.
- Evaluate *DeLorean* on six RVs - 4 real systems, and 2 simulated systems in a wide range of scenarios including severe external disturbance and strong SDAs that targets all the sensors. We compare *DeLorean*'s recovery to prior work on attack recovery in RVs, namely SSR [27] and PID-Piper [30].

Our results are as follows. (1) *DeLorean* recovers RVs from SDAs, and achieves mission success in 90.7% of the cases on average, while prior work is only effective when at most 1 or 2 sensor types are attacked. Furthermore, *DeLorean* achieves 73% mission success in the worst case scenario i.e., when all sensors are attacked under extreme environmental disturbance. (2) *DeLorean* successfully recovers RVs from adaptive attacks (i.e., the attacker knows *DeLorean*'s recovery

strategy and deliberately crafts attacks to deceive it), and (3) *DeLorean*'s attack diagnosis has 100% true positives, and 10% false positives. In the case of false-positives, the diagnosis triggers gratuitous recovery, and the RV successfully completes the mission.

## II. BACKGROUND AND THREAT MODEL

In this section, we present an RV's state estimation process. Then, we present sensor deception attacks (SDA), and the threat model.

### A. State Estimation and Control in RVs

An RVs' state estimation and control process operates in a feedback loop. It uses the sensor measurements to determine the current physical state of the vehicle, and derive actuator signals for positioning the vehicle in the next state. For example, GPS measures the RV's position, gyroscope measures angular velocity, accelerometer measures velocity and acceleration, magnetometer measures the heading direction, and barometer measures the altitude based on pressure change. In addition, RVs use state estimation and sensor fusion algorithms to enhance the physical state results based on multi-sensor measurements.

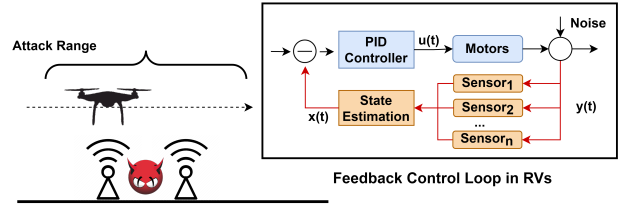


Fig. 1: State Estimation and Feedback Control in RVs. SDA influencing RV's state estimation and control.

Typically a PID (Proportional-Integral-Derivative) controller (Figure 1) is used to regulate the RV's position, velocity and orientation. The PID controller takes the error in the RV's current state and the target state as input, and adjusts P, I, and D gain parameters ( $K_p, K_i, K_d$  in Equation 1) to derive actuator signal such as motor speed, to minimize the error. Summing up those three components, the PID controller derives appropriate actuator signals [41].

$$u(t) = K_p e(t) + K_i \int e(t) dt + K_d \frac{de}{dt} \quad (1)$$

The three terms of the PID controller have different functions: The Proportional (P) term calculates the error between the RV's current state and the target state, and then adjusts the actuator signal based on the magnitude of this error. For example, if the RV is far from the target position, the P term will increase to move the RV towards the target position. The Integral (I) term calculates the accumulated error over time and adjusts the actuator signal based on this accumulated error. The I term is useful in situations where there is a steady-state error in the system that is causing the RV to drift away from the target state. The Derivative (D) term calculates the rate of change of the error and adjusts the actuator signal based on this rate of change. The D term is useful in situations where the RV is moving too fast or too slow towards the target state.

## B. Sensor Deception Attacks

Physical attacks that manipulate sensor measurements from an external source via physical channels have been demonstrated in RVs. e.g., gyroscope measurements can be manipulated through acoustic noise injection [51], and GPS measurements can be manipulated by transmitting false GPS signals [38]. Such attacks are launched by injecting false data to sensor measurements [28], [29], [46].

In this paper, we consider a strong form of physical attacks against RVs - we call these *Sensor Deception Attacks* (SDA). In this attack, one or more sensors in the RV are compromised simultaneously, even up to all the sensors. An SDA is launched by injecting malicious signals to the RV's sensors. For example, an adversary can set up a fake GPS emitter, acoustic signal injectors, and magnetic signal injectors at a geographical location, and target the GPS, gyroscope, accelerometer and magnetometer sensors simultaneously during an RV mission. Such an SDA can be debilitating for the RVs, as it *simultaneously* corrupts the physical properties measured by different types of sensors on the RV (e.g., position, velocity, acceleration, angular velocity, heading direction etc.)

SDAs targeting multiple sensor types have been demonstrated against bare metal systems [44] and self-driving cars [24]. For example, Nashimoto et al. [44] showed that an adversary can target gyroscope, accelerometer, and magnetometer sensors at once through acoustic and magnetic signal injection to influence state estimation even in the presence of sensor fusion (EKF). We demonstrate later that such an attack can crash a drone almost immediately.

**Limitations of Existing Techniques** Existing model-based attack recovery techniques for RVs, PID-Piper [30] and SSR [27], can recover the RV only when a single sensor, or redundant sensors of the same type are attacked simultaneously. Thus, they cannot recover from SDAs that target multiple sensors of different types simultaneously (e.g., GPS, gyroscope and accelerometer).

As RVs are often deployed in critical missions, ensuring safety of the vehicle and the stakeholders is paramount. Therefore, recovery techniques must be resilient to even the worst possible attack i.e., SDAs in which all the sensors are attacked simultaneously. *We define a successful mission as one in which the RV reaches the planned destination without crashing despite SDAs.*

## C. Threat Model and Assumptions

We focus on physical attacks that maliciously perturb one or more of the RV's sensors measurements. To launch the attacks, attackers can deploy signal emitters in locations of their choosing (Figure 1). The attacker can also manipulate any number of RV sensor readings to her desired values, and at any time during the RV's mission.

**Assumptions** We assume that the effects of the signal emitters are limited to a range (distance between emitter and RV). This is because malicious GPS signal emitters, acoustic signals etc. are only effective up to a certain distance [39], [54]. We further assume that the attacker's locations are fixed, and they can place signals emitters at a few locations along the RV's path (but not all along it). However, the attacker cannot follow the

RV. This is because it is difficult to move the emitters relative to the target RV, and still interfere at the natural frequency of the sensors to cause resonance [54], which is necessary for the attack's success. Prior work on physical attacks has also used only static signal emitters [39], [51], [53], [54].

We do not consider obstacles in our experiments, which is in line with almost all the prior work in this area [27], [28], [30], [46]). This is because the RV's trajectory planning can be equipped with complementary obstacles or collision avoidance components if obstacles are expected in the mission [42]. We have explained in Section VII how DeLorean can be extended for obstacle avoidance.

We also assume that the RV's starting position is an attack-free zone. This is because the RV needs to gather some attack-free historical state information to enable replay by our technique. Finally, we assume that the attacker does not have the ability to control the RV's environmental conditions, e.g., wind, friction etc.

## III. INITIAL STUDY

We perform an initial experiment to understand how sensor perturbations due to SDAs propagate in the RV's feedback control loop. We then derive the requirements for the recovery technique.

### A. Experiment

We launch an SDA targeting *all* the onboard sensors of a Sky-viper drone i.e., GPS, gyroscope, accelerometer, magnetometer, barometer (drone system details are in Section VI). In this experiment, we run a simple mission and issued the following commands: 1) Take-off, attain an altitude of 10 m, (2) Navigate in a straight line and cover a distance of 50m, and (3) Land, when the target is reached. We launch the SDA once the drone navigates towards its target in a straight line (i.e., steady state). We intermittently launched 4 instances of SDA at  $t=10s$ ,  $t=20s$ ,  $t=35s$ , and  $t=45s$ , targeting all the onboard sensors. We deliberately perform the SDAs intermittently to understand the correlation between sensor manipulations, behaviour of the PID controller and corruption of actuator signal. The first 3 instances of SDA lasted for 2s, whereas, the fourth instance of SDA lasted for more than 5s, which caused the drone to crash.

Figure 2 shows the impact of the attack. Figure 2a shows the error inflation in roll and pitch angles. For simplicity, we show only 2 physical states of the RV. Figure 2b shows the PID controller's proportional (P) gain values. For simplicity we show only 1 out of the 3 terms of the PID controller. Figure 2c shows the drone's actuator signal. Again, we show only the actuator signals of 2 out of 4 motors in the drone i.e., the Pulse Width Modulation (PWM) values for M1 and M2 in Figure 2c, which are almost identical.

Recall that the PID controller takes the error between the RV's target and current physical states ( $e_s = target - current$ ) as input, and derives the appropriate actuator signal (Figure 1). The PID controller adjusts the P, I, and D gain parameters to derive actuator signals as per the error  $e_s$ . For example, in Figure 2b when the drone was issued the takeoff command (at  $t=0$ ), the PID controller adjusted the P gain to increase the

PWM output for takeoff (at  $t=0$  in Figure 2c). After attaining an altitude of 10m, the drone was issued a command to navigate 50m in steady state. Because the  $e_{roll}$  and  $e_{pitch} \approx 0$  (Figure 2a), the P gain is set to 2.4 to derive appropriate actuator signals for a steady state flight. In the attack free segment of the mission (green boxes), the trend in P gain is coherent and the actuator signals is derived as:  $P * (e_s) + I_{term} + D_{term}$ .

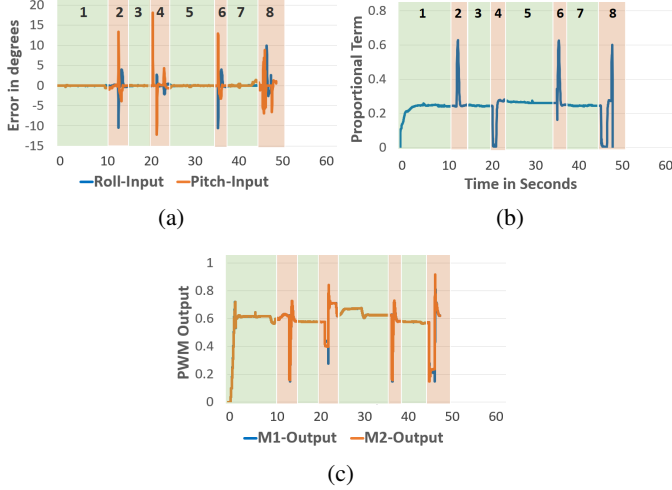


Fig. 2: Impact of SDA, (a) Error inflation in RV's physical state. (b) Fluctuation in Proportional term, (c) Fluctuations in RV's actuator signal. Green parts show the values in absence of SDA, Red parts show values (fluctuations) under SDA.

Under an attack, the sensor manipulations propagate in the drone's control loop and corrupt its state estimations (Figure 1). This leads to fluctuations in the error  $e_s$ , as shown in Figure 2a i.e.,  $e_{roll}$  and  $e_{pitch}$  increases at  $t=10$ ,  $t=20$ ,  $t=35$  and  $t=45$  (shown in red boxes). Due to the error inflation, the PID controller adjusts the P gain ( $PWM = \uparrow P * (e_s)$ ) in an attempt to minimize  $e_s$  as shown in Figure 2b, which in turn leads to the actuator signals fluctuating. As shown in Figure 2c, starting  $t=45$ , the PWM values of M1 and M2 fluctuate between 0.2 and 0.9, which results in a crash of the drone eventually. *Thus, attack induced sensor perturbations corrupt the PID controller's operations, resulting in uncontrolled fluctuations leading to unsafe actuator signals.*

### B. Recovery Requirements

Based on the above experiment, we derive two requirements for recovering RVs from SDA: **R1** Prevent attack induced sensor manipulations from propagating in the RV's feedback control loop, and control the corruption of the PID controller's inputs and PID gain parameters. **R2** Derive safe actuator signals to maneuver the RV out of the attack zone.

Our recovery approach contains two steps: First, we isolate the sensors under attack from the feedback control loop via attack diagnosis. This prevents the corrupted sensor measurements from propagating in the RV's feedback control loop (satisfying **R1**). Second, we replay the historic physical states corresponding to the targeted sensors till the RV is out of the attack zone. The historic states consist of the RV's position

$(x, y, z)$ , velocity  $(\dot{x}, \dot{y}, \dot{z})$ , acceleration  $(\ddot{x}, \ddot{y}, \ddot{z})$ , Euler angles  $(\phi, \theta, \psi)$ , angular velocities (rotation speed of the motors  $\omega_\phi, \omega_\theta, \omega_\psi$ ), and magnetic fields  $(x_m, y_m, z_m)$ . We record the RV's relative position (distance traveled).

Because attacks result in erratic error inflation in RV's physical states, the PID controller, in an attempt to minimize the error ends up over-compensating (persistently adjusts P gain as shown in Figure 2b) [30], which results in erroneous actuator signals. By replaying (safe) historic states to the RV's PID controller, the error  $e_s$  between RV's target state and current physical state is controlled (e.g., instead of erratic fluctuations, the position error shows steady trends as the RV progresses in the mission, and the error in the angular orientation remains constant) regardless of the external disturbance (examples in Appendix X-B). In other words, due to the historic state replay, the PID controller presumes that the RV is behind in the mission trajectory, and the PID controller sets appropriate Proportional (P) gain parameters to derive actuator signals to close the gap between the current state and the target. Replaying historic states eliminates P gain overcompensation and PID controller derives safe actuator signals (satisfying **R2**).

For example, in Figure 2, we record the RV's physical states during the attack-free phase of the mission (shown in green boxes). When SDA is detected at  $t=45$ s, we identify the targeted sensors, and replay the safe historic states recorded in phase **7** corresponding to the targeted sensors. For example, if the gyroscope sensor is under attack, we replay the historic physical states calculated using gyroscope measurements e.g., roll, pitch and yaw angles.

## IV. DESIGN

This section presents the *DeLorean* framework Figure 3 shows the *DeLorean* framework running onboard the RV. *DeLorean* uses an existing attack detector to detect attacks, and performs diagnosis and recovery after detection. Note that *DeLorean* is agnostic of the attack detection technique, and can use any attack detection technique proposed for RVs [28], [30], [46]. Such attack detectors are shown to be effective in detecting attacks (i.e., have low false negatives). The attack detector distinguishes the malicious events from non-malicious disturbances. Only when the attack detector indicates an attack, does *DeLorean* activate diagnosis and recovery.

*DeLorean* has two main innovations: (i) **Attack Diagnosis**: Under an attack, *DeLorean* identifies the targeted sensors to selectively apply the corrective measures, and (ii) **Historic State Replay**: *DeLorean* replays historic states recorded from an attack-free phase of the mission to control corruption of PID controller's operations and derive safe actuator signals under attacks. In the attack-free phases of the RV mission, we record the sequence of historic states in a sliding window. *DeLorean*'s operations are shown in Figure 3.

Figure 4 shows the components of *DeLorean*. **1** A canonical attack detector uses the sensor measurements  $y(t)$  to derive the RV's next physical state  $x'(t)$ , and compares it with the values derived by the state estimation module  $x(t)$ . If the residual  $r = |x'(t) - x(t)|$  exceeds a predefined threshold, that indicates an attack [28], [30], [46]. Once an attack is detected, **2** the *Recovery Switch* activates the **3** *Attack Diagnosis* to identify the sensors targeted by the attack, and isolates the

targeted sensors from the feedback control loop. This prevents the attack induced sensor manipulations from propagating and causing cascading errors in the RV's feedback control loop.

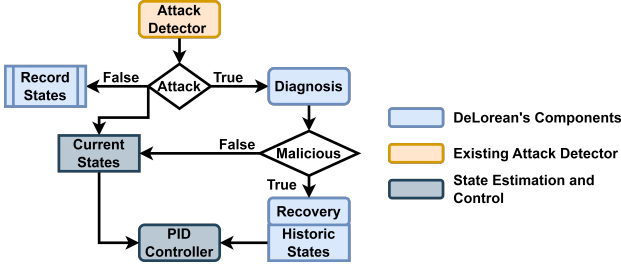


Fig. 3: Sequence of operations in attack detection, diagnosis and recovery. These operations run onboard the RV.

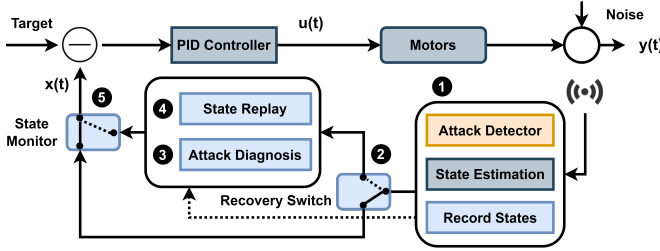


Fig. 4: Feedback control loop with recovery modules

However, simply removing a stream of inputs from the feedback control loop will disrupt the PID controller's operations and will result in erroneous actuator signals. Therefore, the ④ *State Replay* modules *replays* a sequence of historic states corresponding to the isolated sensors, which provides the needed feedback ⑤. Finally, the *State Monitor* forwards the physical states  $x(t)$  to the PID controller, after substituting the attacked sensors with their corresponding historical states, until the attack subsides. The PID controller, using the selectively replayed historic states derives safe actuator signals, and maneuvers the RV out of the attack zone.

Recall that the Integral (I) and Derivative (D) terms in the PID controller update gain parameters based on accumulated error and rate of change of error respectively between the RV's current and target states. As a result of historic state replay, the accumulated error will increase and the rate of change of error may increase depending on the RV's trajectory. This may affect the PID controller's stability when *DeLorean* switches from historic states to sensors after the attack subsides. To prevent any disruptions, during historic state replay, we stop updating the I and D terms' internal states, and we resume them when *DeLorean* switches back to sensors.

#### A. Attack Diagnosis

The first step in *DeLorean* is to identify the targeted sensors once an attack is detected. Attack induced sensor manipulations corrupt the RV's physical states that are estimated using the targeted sensors. For example, when the gyroscope sensor is under attack, it leads to the corruption of the RV's Euler angles (roll, pitch, yaw), and angular velocity (Table I shows the states to sensor mapping). We observe that in attack-free segments of the mission, the error between the

RV's past and present physical states is largely constant i.e.,  $e = |state_t - state_{t-1}| = c \pm \epsilon$ , where  $\epsilon$  is environmental noise. However, under attack, the error  $e$  increases i.e.,  $e \gg c$  [28], [30], [46]. Our approach for attack diagnosis is to monitor the inflation in error  $e_i$ , where  $i \in PS$  (all the physical states of the RV, Equation 2) and find the probability that the corresponding sensor is under attack given the observed error  $e_i$ .

$$PS = x, y, z, \dot{x}, \dot{y}, \dot{z}, \ddot{x}, \ddot{y}, \ddot{z}, \phi, \theta, \psi, \omega_\phi, \omega_\theta, \omega_\psi, x_m, y_m, z_m \quad (2)$$

TABLE I: Physical states and corresponding sensors in RVs

Sensors	GPS	Gyroscope	Accel	Barometer	Magnetometer
States	$x, y, z, \dot{x}, \dot{y}, \dot{z}$	$\phi, \theta, \psi, \omega_\phi, \omega_\theta, \omega_\psi$	$\ddot{x}, \ddot{y}, \ddot{z}$	$z$	$x_m, y_m, z_m$

However, error inflation in the RV's physical states can also occur due to the RV's physical dynamics in the mission (e.g., mode changes), and not only due to attacks. Thus, it is important to find the root cause of the error inflation in RV's physical states. We use factor graphs (FG) to monitor the error inflation in physical state. FGs are probabilistic graphical models that allow expressing conditional relationships between variables [23]. In particular, we use FG to represent the causal relationship between the observed error  $e_i$  and find the probability that the corresponding sensor is under attack i.e., the outcome  $s_i$ . We consider binary outcomes for the sensors i.e., *malicious* (targeted by SDA) or *benign* (attack-free).

The causal relationship between  $e_i$  and  $s_i$  can be expressed as a conditional probability problem i.e.,  $P(s_i|e_i)$ . There are two ways to calculate conditional probability: (1) Using a joint probability distribution over the observed  $e_i$ , and the probable outcomes  $s_i$  (i.e., benign or malicious sensors). However, expressing the joint probability distribution at runtime for binary outcome will have high computation and storage overheads. Further, as the mission progresses, the time taken to calculate probabilities will increase exponentially. Therefore, this approach is not practical.

(2) Using a Bayesian approach, we can calculate  $P(s_i|e_i)$  based on the values of known probabilities of  $P(e_i|s_i = \text{malicious})$  and  $P(e_i|s_i = \text{benign})$ . To be able to calculate  $P(s_i|e_i)$ , we will need to run a large number of experiments and profile the observed error  $e_i$  in RV's physical states under attacks as well as in absence of attacks to calculate  $P(e_i|s_i = \text{malicious})$  and  $P(e_i|s_i = \text{benign})$ . This will also not work in our case due to two reasons: First, it is difficult to know how many observations are enough. Second, if we observe an error during inference that was not observed during profiling, the Bayesian approach will assign it a zero probability (i.e., Zero Frequency problem). Thus, even if a sensor is under attack, the Bayesian approach will wrongly conclude the sensor is benign.

In contrast to the above approaches, FGs allow fine-grained representation of the complex joint probability distribution between variables through a product of smaller probability distributions. Thus, they incur low computation and storage overheads. Further, instead of relying on profiling, FGs use functions (i.e., factor functions) to express conditional relationships. Thus, FGs can accommodate unseen observations ( $e_i$ ), and do not suffer from the Zero Frequency problem. This is why we use FGs for attack diagnosis.



Figure 5 shows an example of FG-based diagnosis. The FG represents the relationships between error  $E = (e_1, \dots, e_n)$  and the probable outcome  $S = (s_1, \dots, s_n)$  using a bipartite graph, where  $e_i$  and  $s_i$  are observed error and outcomes of the RV's physical states (Equation 2). Factor functions  $F = (f_1, \dots, f_n)$  define relationships between observed errors ( $e_{i-1}, e_i$ ) and probable outcomes  $s_i$ . Using FG, we calculate the probability of each physical state  $s_i$  being malicious given the observed error  $e_i$  i.e.,  $P(s_i = \text{malicious} | e_i)$ . If certain physical states are found malicious, we deem the corresponding sensors (Table I) are under attack.

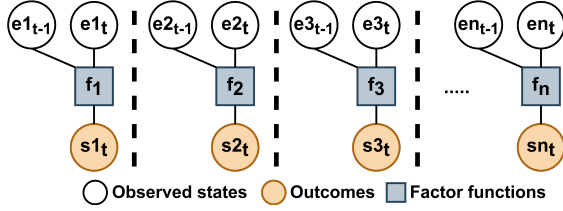


Fig. 5: Factor graph for diagnosing malicious sensors under an SDA given the observed errors in RV's physical states.

**Factor Graph Construction** The steps involved in constructing the FGs and using FGs for attack diagnosis are as follows.

*Step 1 - Express the causal relationships between errors in RV's physical states and the probable outcome using factor functions.* To express such a relationship, the first step is to determine the safe and unsafe ranges of the error  $e$ . We run attack-free missions and collect mission traces, and we observe the variation in error  $e$ . Recall that in an attack free phase, the error is mostly constant  $e = c + \epsilon$ , where  $\epsilon$  is environmental noise. We deem  $e$  to be in the safe range if  $0 < e < \delta$ , where  $\delta = \text{median}(e) + k * \text{stdev}(e)$ . The value of  $\delta$  is RV-specific, and it is derived empirically (details in Section VI).

The factor functions rely on the  $\delta$  values of the respective physical states to output a discrete value representing the possible outcome for each sensor (Equations 3). In particular, the factor function expresses the relations if  $e_{i-1} > \delta$  and  $e_i > \delta$ , then what is the most probable outcome for the sensor (malicious or benign)? Note that we monitor error in past four states ( $e_t = |state_t - state_{t-1}|$ ,  $e_{t-1} = |state_{t-2} - state_{t-3}|$ ) to disregard transient error inflation and benign physical dynamics changes in the mission.

$$f_i(e_{i-1}, e_i, s_i) = \begin{cases} 1, & e_i > \delta \text{ and } e_{i-1} > \delta \text{ and if } s_i = \text{malicious} \\ 0, & \text{otherwise} \end{cases} \quad (3)$$

*Step 2 - Construct per sensor factor graphs.* We repeat Step-1 and construct FGs expressing relationships between the observed errors  $e_i$  and the probable outcomes  $s_i$  for all the physical states corresponding to all the sensors of the RV. The factor functions shown in Equation 3 is used for this purpose (only the value of  $\delta$  changes, which is empirically determined).

*Step 3 - Perform inference on the factor graphs to diagnose the targeted sensors.* We feed the physical states derived from sensor measurements to the per sensor FGs to determine the targeted sensors. We calculate the probability of  $s_{i_t} = \text{malicious}$ , for all the physical states PS (Equation 2) given the observed  $e_{i_{t-1}}, e_{i_t}$ . The joint probability distribution can

be factorized as:

$$P(E_t, S_t) = \prod_{i=1}^n f_i(e_{i_t}, e_{i_{t-1}}, s_{i_t}), i \in PS \quad (4)$$

Thus, at each time  $t$ , the conditional probability is

$$P(s_{i_t} = \text{malicious} | e_{i_t}) = \prod_{i=1}^n f_i(e_{i_t}, e_{i_{t-1}}, s_{i_t}), i \in PS \quad (5)$$

We assume that each sensor is equally likely to be in a benign or malicious state initially, so  $P(s_i = \text{benign}) = 0.5$  and  $P(s_i = \text{malicious}) = 0.5$ . We use Maximum Likelihood Estimation (MLE) to find the likelihood of each possible outcomes of  $s_i$  given the observed errors  $e_i$ . Because the observed  $e_i$  inflates under attacks, the  $P(s_i = \text{malicious}) > P(s_i = \text{benign})$ . We deem those states to be malicious where  $P(s_{i_t} = \text{malicious}) > 0.5$ , and deem the corresponding sensors (Table I) as being under attack.

### B. Historic State Replay for Recovery

When the RV is in an attack free phase, we record the sequence of physical states estimated from all the on-board sensors in a sliding window. Figure 6a shows the details. The physical states at time  $t$  are represented as  $x(t)$ , and the historic physical states recorded in a window are represented as  $HS$  (states shown in Equation 2).

At each time  $t_w$  since the start of the RV's mission, if no alert is raised by the attack detector (Figure 3), starting at  $t_w$  we record  $x(t)$ . We save the  $HS$  recorded in window  $w_i$  and proceed recording states in the next window  $w_{i+1}$ . At the end of window  $w_{i+1}$ , we discard the  $HS$  recorded in the previous window  $w_i$ . If we detect an attack however, we stop the recording, and discard the states recorded in the current window  $w_i$  as these may be corrupted by the attack (Figure 6b). We replay the  $HS$  recorded in the previous window  $w_{i-1}$  for recovery which is attack-free (as no alert was raised by the attack detector), and is hence uncorrupted.

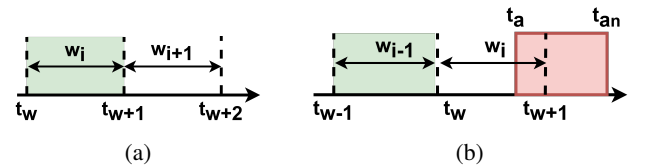


Fig. 6: (a) Recording historic physical states in a sliding window. (b) Ensuring historic states are attack-free.

However, it is possible for an attack to be stealthy and span multiple sliding windows [29], in which case, it will be challenging to ensure an attack-free  $HS$  for recovery. Such stealthy attacks can inject seemingly benign and controlled bias in the sensor measurements over a long time, thereby evading detection, and causing disruption in the RV's mission. Many attack detection techniques such as Savior [46] and PID-Piper [30] detect stealthy attacks using cumulative sum statistics (CUSUM). However, there is necessarily a delay in attack detection i.e., the time interval between the onset of the stealthy attack and the time when the attack detector raises an alert. Due to the detection delay, *DeLorean* might record corrupted

*HS* for recovery, which it incorrectly deemed safe as no alarms were raised by the attack detector. Therefore, to handle stealthy attacks, we empirically determine the window length to be large enough so that stealthy attacks can be detected within a single sliding window (details are in Section V-A).

Another challenge is that sensors in RVs are sampled at different rates e.g., the sampling rate for gyroscope is 400 Hz, whereas, the sampling rate for Barometer is 100 Hz. It is important to align the data streams when recording the historic states. To address this problem, we select a single target frequency for recording the *HS*, which is the highest sampling rate of all the sensors. We then align the low frequency streams with the high frequency streams by inserting additional data points in the low frequency stream to match the sample points in the high frequency streams. In particular, we duplicate the last data point in the low frequency streams based on the ranges of the sample points of the high frequency streams.

### C. Algorithm

Algorithm 1 shows *DeLorean*'s algorithm for attack diagnosis and recovery. In the absence of attacks (based on the attack detector's response), *DeLorean* records the physical states associated with all the on-board sensors (Lines 7-15) in a sliding window. Once the attack detector raises an alert, *DeLorean* activates recovery mode (Line 17). First, it stops recording, and prepares the most recent safe *HS* for recovery. Then, it activates the diagnosis procedure (Line 20). The attack diagnosis module determines the sensors under attack, if any, using FGs (Line 27-33). Once the targeted sensors are determined, *DeLorean* identifies the corresponding physical states, and replays the historic states only for the identified sensors in the RV's control loop. Once the attack subsides (based on the attack detector's response), the recovery mode is turned off.

Due to the recovery, if the RV has veered off from the planned trajectory, *DeLorean* finds a desired route to the destination, and sends the new path to the autopilot for course correction (not shown in algorithm). Due to space constraints, we show the algorithm for course correction in Appendix X-E - this algorithm will be activated if the RV has veered off from its path due to *DeLorean*'s recovery.

### D. Course Correction

Because *DeLorean* replays historic states to derive constant (or non fluctuating) actuator signals for safely maneuvering the RV under SDA, it may cause the RV to veer off its planned trajectory. For example, in Figure 7a, the RV was supposed to turn left in the attack zone. However, because of the attack and subsequent recovery, the RV will miss the turn and continue straight. To address this issue, we add a course correction component that recalculates the RV's trajectory to reach its destination, after it leaves the attack zone. The course correction component will also avoid the path taken by the RV out of the attack zone to avoid reentering the attack zone. More details about the course correction are in Appendix X-E.

There is one corner case in the course correction procedure where the RV might miss its destination. If the RV's destination is itself in the attack zone, due to recovery activation, the RV will keep moving forward instead of completing the mission.

### Algorithm 1 Algorithm for Attack Diagnosis and Recovery

```

1:  $w \leftarrow$  historic state recording window
2:  $S \leftarrow$  historic physical states used for recovery
3:  $Tx \leftarrow$  physical states corresponding to targeted sensors
4: procedure HISTORICSTATEPLAY
5:    $alert \leftarrow AttackDetector()$ 
6:   while ! $mission\_end$  do
7:     if ! $alert$  then ▷ recording historic states
8:        $recovery\_mode \leftarrow false$ 
9:       if  $t_w < t_{w+1}$  then
10:         $record \leftarrow true$ 
11:         $w_i[.] \leftarrow x(t)$ 
12:       else
13:         $delete\ w_{i-1}$ 
14:         $t_w = t_{w+1}$ 
15:       end if
16:     else
17:        $recovery\_mode \leftarrow true$  ▷ recovery activated
18:        $record \leftarrow False$ 
19:        $HS = w_{i-1}$ 
20:        $targetedSensors \leftarrow Diagnosis()$ 
21:        $Tx \leftarrow targetedSensors$ 
22:        $Tx[.] \leftarrow HS[.]$  ▷ replaying for targeted sensors
23:     end if
24:   end while
25: end procedure
26: procedure DIAGNOSIS
27:   while ! $mission\_end \forall sensors\ do$ 
28:      $e = |(e_t) - (e_{t-1})|$ 
29:      $s_t \leftarrow argmaxP(s_t|e)$  ▷ most probable outcome
30:     if  $s_t = 1$  then
31:       return  $malicious$  ▷ targeted sensors
32:     end if
33:   end while
34: end procedure

```

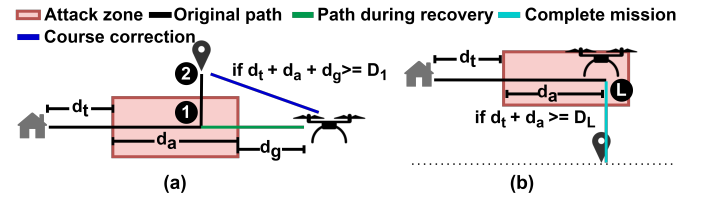


Fig. 7: (a) Course correction after the RV is out of the attack zone. (b) *DeLorean* recovery when the destination itself is in the attack zone.  $D_w$  = distance to waypoint  $w$ ,  $d_t$ : distance traveled before attack,  $d_a$ : distance traveled under attack,  $d_g$ : distance traveled after exiting attack zone.

To handle this scenario, when recovery is activated, we check if the distance traveled without attack  $d_t$  and under attack  $d_a$  is distance to destination  $D_L$  (final waypoint). If so, the RV has reached near its target, and the mission is completed. Figure 7b illustrates this scenario.

## V. EXPERIMENTAL SETUP AND ATTACK PARAMETERS

In this section, we present our experimental setup, metrics, and attack parameters for evaluating *DeLorean*. We then present *DeLorean*'s parameters derived from our experiments.

**Subject RVs** To evaluate *DeLorean*, we use six RV systems. Four of these are real RVs. These are shown in Figure 8 (from the left) (1) Pixhawk based DIY drone [43] (Pixhawk drone), (2) Tarot 650 drone [15] (Tarot drone) (3) Aion R1 ground rover [3] (Aion rover), and (4) Sky Viper Journey

drone [13] (Sky-viper drone). The first three RVs are based on the Pixhawk platform [43]. The Sky-viper drone is based on an STM32 processor. These RVs are all equipped with the following five sensors: GPS, gyroscope, accelerometer, barometer and magnetometer, but each RV has different numbers of individual sensors (Table II). The other two RV systems are simulated RVs, (4) Ardupilot’s quadcopter (ArduCopter), and (5) Ardupilot’s ground rover [5] (ArduRover). We use the APM SITL [5], and Gazebo [8] platforms for vehicle simulations.



Fig. 8: Real RV Systems (a) Pixhawk drone, (b) Tarot drone, (c) Aion Rover, (d) Sky Viper drone.

**RV Controller** Our approach is designed primarily for PID controllers. This is because almost all the open source as well as commercial autopilot for RVs use the PID controller e.g., Ardupilot [5], PX4 [12], Paparazzi [10], and simple-flight [2].

**RV Missions** We run a diverse set of 340 missions with varying mission duration, and mission distances. We simulate a wind flow between 0-10 m/s to vary the environmental conditions. The mission paths emulate various real-world RV missions: (1) a last mile delivery drone [37] (straight line path, polygonal path), (2) drones used for surveillance or agriculture [1] (circular or polygonal path), and (3) rovers deployed in warehouse management [4] (polygonal paths). More details about RV mission path is in Appendix X-F.

**Comparison** We quantitatively compare our results with both SSR [27], and PID-Piper [30], which are the only other recovery techniques for RVs. Because SSR is not publicly available, we implemented it using Matlab’s system identification (SI) tool [14] with our best effort. We collected RV mission traces (training and testing sets) and derived the system model using the training set. We validated the software sensor’s accuracy with the testing set. For PID-Piper, we used the publicly available implementation released by the authors [11]. For a fair comparison, we used the Autopilot and simulation platforms that were used by SSR and PID-Piper.

**Success Metric** As done by prior work [30], we consider a mission to be successful, if upon completion, the total deviation from the original destination is *less than 10m*. Most GPS sensors used in commodity RVs have an offset of 5 meters [48]. We consider  $2X$  of the GPS offset as our threshold i.e., 5m offset from the RV’s position, and 5m offset from the destination. This threshold is indistinguishable from the standard GPS error [9]. We consider the mission to be unsuccessful if the RV crashes (physically damaged) or stalls (freezes or stops moving towards the destination). We do not evaluate the effectiveness of the attack detector as we use an attack detector proposed by prior work [30] (hence, out of our scope).

**Runtime Overheads:** We measure the overheads in CPU times, battery consumption, and memory incurred by the RV due to *DeLorean*. As the overheads in simulated RVs depend on the simulation platform, we report the overheads only for the real RVs. For CPU overheads, we measure the CPU times

incurred by the autopilot modules with and without *DeLorean*. During recovery, due to the historic state replay performed by *DeLorean*, the RV’s motor rotation rates increase. We call this the operational overhead. We estimate the battery overhead of *DeLorean* based on both the CPU overhead and the operational overhead. Finally, we estimate the memory overhead for storing the historic states for replay.

#### A. Attack Parameters

**Attacks** As we did not have access to special equipment (e.g., noise emitter, sound source, amplifier, etc.) for mounting physical attacks, we emulated the attacks through targeted software modifications, similar to what most prior work has done [27], [28], [30], [46]. Our attack code interfaces with the sensor libraries in the RV, and manipulates sensor measurements by adding a bias to them (i.e, false data). When an attack command is initiated, the bias values are automatically added to the raw sensor measurements. We derive the attack parameters i.e, bias values, attack range and attack duration to mimic physical attacks via software as closely as possible.

**Sensor Bias Values** We use variable bias values for each sensor within the allowable limit to cause the maximum damage. We derive bias values as per the respective sensor specifications. Table II shows the details. For example, the update frequency of the GPS module used in many industrial and commodity RVs is 0.1s, and the operational limit in its velocity is 500 m/s [16]. Therefore, the maximum hopping distance of the GPS receiver is 50m (update frequency  $\times$  maximum velocity). Thus, for GPS, we set the bias value to be between 5-50m, which is the operating limit of the GPS sensor. Table II shows the bias values used for each sensor.

**Attack Range** We derive the maximum attack range based on prior work that performed the respective attacks through signal injection [44], [45], [52]. We extrapolate their results considering the largest available signal source and amplifier to derive the maximum attack range for each sensor. We found that the optimal attack range for individual sensors is within 26 – 200m. Of all the sensors, the GPS has the maximum attack range [52] of 200m. *Thus, we select 200m as the attack range in our experiments i.e, we assume that attackers can manipulate all the sensors in a 200m range.* This is a stronger assumption than that made in all the prior work [51], [54].

**Attack Duration** We calculate the attack duration based on the time taken by each RV to cover the attack range distance. The RVs in our experiment all travel at a velocity of 10m/s speed, and thus, they take about 20s to cover 200m. *Therefore, we set the maximum duration of an individual SDA to 20s.*

TABLE II: Subject RVs in Evaluation, Number of Sensors, Attack parameters. P: Pixhawk drone, T: Tarot drone, S: Sky-viper drone, AC: ArduCopter, R1: R1 rover, AR: ArduRover

Sensor Type	Number of Sensors						Bias Values	Max Range
	P	T	S	AC	R1	AR		
GPS	1	1	1	1	1	1	5-50m	200
Gyroscope	3	3	1	3	3	3	0.5-9.47 rad	100
Accelerometer	3	3	1	3	3	3	0.5-6.2 rad/s <sup>2</sup>	26
Magnetometer	3	3	1	1	3	1	180 deg	-
Barometer	1	2	1	1	1	1	0.1 kPa	-
Window Size	15.5s	15s	17s	15.5s	18.5s	17s		



## B. DeLorean Modules and Parameters

**Attack Detector** As mentioned, *DeLorean* is agnostic of the attack detection technique, and provides attack diagnosis and attack recovery after the attack is detected. For attack detection, we choose PID-Piper’s publicly available attack detection module [11], as it represents the state-of-the-art and has a high detection rate.

**Attack Diagnosis** We developed the diagnosis module in Python. The module monitors the error  $e$  between the past and present states of the RV. Recall that in the attack-free phase,  $e$  remains within  $0 - \delta$ . We use the standard deviation method to derive the value of  $\delta$  i.e.,  $\delta = \text{median}(e) + k * \text{stdev}(e)$  i.e., if the error  $e$  is more than  $k$  standard deviations away from the mean, it is likely to be an outlier (due to the attack) [47]. We collect attack-free RV mission traces (on both simulated and real RVs with diverse mission trajectories), and empirically determine that  $k = 3$  ensures  $0 < e < \delta$  in the attack-free phase of the mission. We run between 15-25 attack-free missions for each RV to derive the  $\delta$  values, and we validated  $\delta$  values (i.e.,  $e \in 0 - \delta$ ) by running another 15 missions. The one time cost for calculating  $\delta$  values for each RV is 60 minutes (on average). The  $\delta$  values for all the subject RVs are presented in Appendix X-D.

**Attack Recovery** The attack recovery module was developed in C++. Recall that the window size must be large enough that a stealthy attack can be detected in a single sliding window (Section IV-B). Therefore, to find the appropriate window size, we launched stealthy attacks on PID-Piper’s attack detector. PID-Piper uses CUSUM to detect stealthy attacks [29]. Our goal is to identify the maximum duration that the attacker can cause disruptions in the RV mission by launching stealthy attacks while evading detection.

To determine the window size, we launched three kinds of stealthy attacks in all the subject RVs: (1) targeting all the sensors persistently, (2) targeting all the sensors intermittently, (3) targeting each sensor individually. We find that when all the sensors are manipulated persistently, the stealthy attack is detected in under 3.3s. When launched intermittently, the stealthy attack is detected in under 10s. When launched targeting individual sensors, the stealthy attacks against GPS remain undetected for the maximum duration i.e., around 15 – 18s. Therefore, we select the window size for each RV to be larger than the time taken to detect stealthy attacks against the GPS. Table II shows the window size values.

## VI. RESULTS

We first compare the recovery performed by *DeLorean* with other recovery techniques on simulated RVs under SDAs. Then, we present *DeLorean*’s recovery on real RVs, and its performance, memory and energy consumption overheads. We then study the effectiveness of *DeLorean* under environmental disturbances. We also study the need and effectiveness of the attack diagnosis performed by *DeLorean*. Finally, we study *DeLorean* under adaptive attacks.

### A. Comparison of DeLorean, SSR and PID-Piper

We compare *DeLorean* with SSR and PID-Piper in recovering from the SDAs on the simulated RVs. We did not use

the real RVs in this experiment as we encountered crashes in the simulations for SSR and PID-Piper, and hence we did not want to damage the real RVs. We launched 75 missions for each simulated RV protected with SSR, PID-Piper and *DeLorean* respectively. We mounted the same attacks for all three techniques varying the number of sensor types targeted from 1 to 5 (all sensors). Note that when we say a sensor is attacked, we mean that *all* the sensors of that type are attacked.

TABLE III: *DeLorean*’s recovery outcomes compared with SSR and PID-Piper, as a function of the number of sensors attacked. MS: Mission Success, values are in percentages.

# of sensors targeted	SSR		PID-Piper		DeLorean	
	Crash	MS	Crash	MS	Crash	MS
1	20	64	0	100	0	100
2	56	20	64	20	0	100
3	100	0	100	0	0	100
4	100	0	100	0	0	88
5	100	0	100	0	0	82

Table III shows the mission outcomes of *DeLorean*, SSR and PID-Piper under SDAs for different numbers of sensors attacked. From the table, SSR has a mission success rate of 64% for single sensor attacks. However, for attacks targeting two sensors, its mission success rate drops to 20% with a crash rate of 56%. PID-Piper, on the other hand, is 100% effective when only a single sensor is targeted. However, its mission success rate also drops to 20%, and its crash rate increases to 64% when two sensors are attacked. Furthermore, when 3 or more sensors are attacked, both SSR and PID-Piper incurred a 100% crash rate (0% success). Thus, *both SSR and PID-Piper incur crashes and mission failures* for multi-sensor SDAs, and had average mission success rates of 17% and 24% respectively.

In contrast, *DeLorean* incurs *no crashes* in any of the attacks even when all sensors are targeted. *DeLorean* achieves 94% mission success rate on average across all sensor numbers, which is  $\approx 4X$  higher than the mission success rates of both SSR and PID-Piper. In fact, *DeLorean* achieves 100% mission success when 3 or fewer sensors are targeted. Even when all sensors are targeted, *DeLorean* achieves 82% mission success. Thus, *DeLorean* is highly resilient to multi-sensor SDAs.

### B. DeLorean Recovery in Real RVs

We also evaluate *DeLorean* on the four real RVs in various scenarios. From the simulation results, we found that RVs protected with *DeLorean* incurred no crashes during simulation, and so we do not have to worry about damaging the RVs (this was also confirmed by our experiments). Table IV shows *DeLorean*’s recovery outcomes.

Due to space constraints, we only consider two cases: (1) single sensor SDAs, and (2) multi-sensor SDAs that target all the sensors (i.e., the worst case). We find that for both single sensor and multi-sensor SDAs, *DeLorean* incurred *no crashes*. Further, *DeLorean* achieves 100% mission success for single sensor SDAs, and a mission success rate between 80 and 90% (average of 86.25%) for multi-sensor SDAs. These results are comparable to the results of *DeLorean* on the simulated RVs.

TABLE IV: *DeLorean* recovery under SDAs (single sensor and all sensors) on real RVs. CPU, battery, and memory overheads

RV Type	Recovery success rate (%)		CPU Overhead	Battery Overhead	Memory Overhead
	Single	All Sensors			
Pixhawk	100	85	8.8%	22%	0.47 MB
Tarrot	100	90	6.7%	18.75%	0.45 MB
Sky-viper	100	80	9.2%	20%	0.52 MB
Aion R1	100	90	5.5%	14.4%	0.56 MB

Furthermore, even for the failed missions, the deviation from the target was very small (15.6m on average).

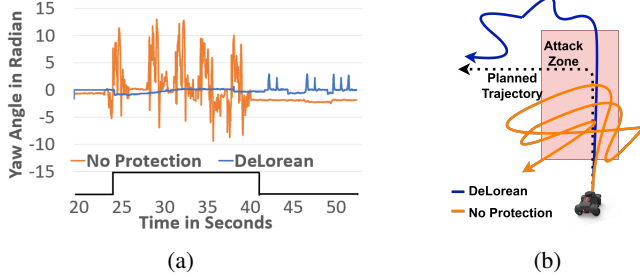


Fig. 9: *DeLorean*'s recovery in Aion rover under SDAs. (a) Yaw angles with and without *DeLorean*, SDA launched 25-40s (bottom graph). (b) Rover's trajectory under recovery.

Figure 9 shows *DeLorean*'s recovery on the Aion rover. In this mission, the rover should head straight and make a left turn. Figure 9b shows the mission trajectory under an SDA targeting all the sensors from 25s to 40s (shown in the bottom part of the figure) without any protection. As can be seen in Figure 9a, without *DeLorean*, the rover's yaw angle estimates suffer heavy fluctuations (between -10 and +15 radian), which should be constant without attack. As a result, the rover follows a bizarre path (Figure 9b), and does not reach its destination, resulting in mission failure.

However, when *DeLorean* is deployed on the Aion rover, it prevents the yaw angle fluctuations due to the attack (Figure 9a). As a result, the rover navigates itself out of the attack zone. However, due to the attack, it missed the left turn it was supposed to execute (Figure 9b). Therefore, *DeLorean*'s course correction component successfully navigates the RV towards the target by calculating a new path. The small spikes in yaw angles with *DeLorean* in Figure 9a are due to the RV adjusting its position and heading direction to follow the new path (curly blue lines in Figure 9b). However, due to course correction, the RV covers a larger distance and the mission duration increased by 1.5X. Thus, *DeLorean* safely recovers the rover from the SDA, and results in mission success.

### C. Recovery under Environmental Disturbance

There are different kinds of environmental disturbance that RVs may encounter. We use wind as a representative of environmental disturbances, and evaluate *DeLorean* under wind conditions to understand the effect of environmental disturbances on recovery. We used simulation in this experiment, as we cannot control wind speeds in the real world. We simulate different wind conditions (Beaufort scale [6]) i.e., low

wind (0-5m/s), moderate wind (5-8m/s) and strong wind (8-10m/s), and we test *DeLorean*'s recovery under single and multi sensor SDAs (all sensors) in ArduCopter. Wind speeds exceeding 10 m/s are considered unsafe for RVs. In all the missions, the wind flow was opposite to the RV's direction of travel.

To evaluate the effect of environmental disturbance, we consider two scenarios. In the first scenario, wind is present only after the attack, but not before it (Scenario A). In this scenario, the recorded historic states may not represent the RV's action under windy conditions, thus making replay-based recovery inaccurate. In the second scenario, the wind is present both before and after the attack (Scenario B), and the recorded historic states are noisy as a result. We do not present the scenario where wind is present only before attack and not after - we found *DeLorean*'s recovery in this scenario is similar to scenario B where *DeLorean* recorded noisy states.

Table V shows *DeLorean*'s recovery under single and multi-sensor SDA in the two scenarios. We carried out 40 missions for each case. In half of these missions, we launched the above two kinds of attacks, while the other half were attack-free. We normalize the results based on the number of missions that were successful without any attacks under the same wind conditions.

TABLE V: *DeLorean*'s recovery in the three wind scenarios. Scenario A: windy conditions only after the attack, and Scenario B: windy conditions through the mission.

Wind Flow	Single Sensor SDA		Multi Sensor SDA	
	Scenario A	Scenario B	Scenario A	Scenario B
Low	100%	100%	90%	80%
Moderate	100%	94.73%	89.47%	78.94%
Strong	86.67%	80%	80%	73.33%

We find that in low wind conditions *DeLorean* achieves high mission success and no crashes under both single and multi sensor SDAs in both scenarios A and B. In moderate wind conditions, *DeLorean* achieves a recovery success rate of 94-100% for single sensor SDA, and 78-89% for multi sensor SDA. However, in strong wind conditions *DeLorean*'s recovery success rates drops significantly. Under strong wind, *DeLorean*'s recovered the RV in 80-86% of the cases from single sensor SDA. In the worst case i.e., strong wind and multi-sensor SDA, *DeLorean*'s recovered the RV in 73-80% of the cases. Examples of *DeLorean*'s recovery are in Appendix X-H. When all the sensors are under attack, crashes occurred in 4% and 11% of the cases (on average) in scenario A and scenario B respectively.

The reason for *DeLorean*'s recovery not being as effective under moderate and strong wind is that the control actions corresponding to the recorded states are not representative of the correct control actions. This forces the PID controller to fine-tune the P term which sometimes results in erroneous actuator signals (Section III).

### D. Runtime, Memory and Battery Overheads

Table IV shows the runtime and battery overheads incurred by *DeLorean* on the real RVs. The CPU overhead varies from 5.5% to 9.2%, with an average of 7.5% across the four RVs.

This is slightly higher than the CPU overhead incurred by SSR and PID-Piper, which are 6.9% and 6.35% respectively. Furthermore, *DeLorean*'s memory overhead is between 0.45 MB and 0.56 MB across the different RVs. This overhead is less than 3% as our RVs have over 20 MB RAM.

Under attacks, *DeLorean* incurs battery overhead between 14.4% and 22% across RVs (18.87% on average). This battery overhead is due to the operational overhead of increasing the motor speeds due to the replay, which is only incurred when under an attack. Similarly under attacks, the RV missions duration increased by 1.7X (on average) due to the course correction performed by *DeLorean*.

#### E. Need for Attack Diagnosis

To understand if attack diagnosis is needed for recovery from SDAs, we compare *DeLorean*'s recovery with naive replay in recovering RVs. A naive replay technique replays the historic states corresponding to all the sensors regardless of the number of sensors under attack (without any diagnosis). In contrast, *DeLorean* performs attack diagnosis to identify the targeted sensors, and replays only those historic states corresponding to the targeted sensors.

In this experiment, we perform 75 missions each for *DeLorean* and naive replay techniques for the simulated RVs, and launch SDAs targeting 1 to 4 sensors in each mission (all combinations). This is because when all the 5 sensors are targeted, both *DeLorean* and naive replay would be indistinguishable from each other.

TABLE VI: Mission success rate of Naive replay (without diagnosis) and *DeLorean*. No crashes occurred in both cases.

# of sensors targeted	Naive Replay	<i>DeLorean</i>
1	85.33%	100%
2	82.66%	100%
3	82.66%	100%
4	80.00 %	88%

Table VI shows the average mission success rates for each category of missions. We find that both *DeLorean* and naive replay prevented crashes in all the cases. However, *DeLorean* had a much higher success rate than naive replay in all cases. Overall, naive replay resulted in mission success rates between 80 and 85%, while *DeLorean* resulted in much higher mission success rates between 88% and 100%. Further, *DeLorean* achieves 100% mission success when fewer than four sensors are targeted. Finally, even for the failed missions, we find that the average deviation from the target for *DeLorean* is 13.6m, whereas, the average deviation for naive replay is 20.2m. Thus, *diagnosing the attack and selectively replaying historic states achieves higher mission success than naive replay.*

#### F. Effectiveness of Attack Diagnosis

In this section, we investigate the effectiveness of the attack diagnosis by measuring true positives (TP) and false positives (FP). TP is the fraction of times attack diagnosis correctly identified the sensors targeted by SDA. FP is the fraction of times attack diagnosis falsely identified sensors as attacked even in the absence of an attack. We compare *DeLorean*'s diagnosis using factor graphs with a naive diagnosis technique

that only monitors the error in the last step ( $e = |State_t - State_{t-1}|$ ) against the threshold. Our goal is to analyze if we need factor graphs that track multiple past states as used in *DeLorean*, or if the naive diagnosis is enough.

TABLE VII: Comparing the effectiveness of attack diagnosis.

Diagnosis Method	True Positive Rate	False Positive Rate
<i>DeLorean</i> 's Diagnosis	100%	8%
Naive Diagnosis	86%	18%

We run 50 missions on Arducopter and launched the same attacks for Naive and *DeLorean*'s diagnosis to compare them. Table VII shows the results. We find that the Naive diagnosis resulted in 86% TPs. In contrast, *DeLorean*'s diagnosis correctly identified the targeted sensors in all the cases, thereby achieving a 100% TP rate.

To measure the FP rate in diagnosis, the attack detector needs to (falsely) report an attack when there is none. Thus, we emulate a false alarm in the attack detector to study FPs in attack diagnosis. We run 50 missions in ArduCopter. As the diagnosis mechanisms independently analyze errors in the RV's physical states, both Naive and *DeLorean*'s diagnosis reported that no sensors were targeted by the attack in 82% and 92% of the cases respectively, and hence they dismiss the detection as a false alarm.

We find that Naive diagnosis resulted in more than 2X FPs than *DeLorean*'s diagnosis (Table VII). This is because Naive diagnosis monitors the physical states' error only in the last step, and hence fails to account for the benign deviations in RV's physical states. In contrast, *DeLorean*'s diagnosis monitors the sequence of errors in four previous steps (this is inherent to the FG approach, see Figure 5). Thus, FG captures the causality of deviations in RV's physical states to infer if the corresponding sensor is under attack. In 8% of the cases where *DeLorean*'s diagnosis incurred FPs, it led to gratuitous recovery, and achieved mission success in all of them.

#### G. Adaptive Attacks

We evaluate *DeLorean* under three adaptive attacks to test if an adversary who knows *DeLorean*'s recovery strategy can subvert it. The three attacks correspond to attackers who (1) launch SDAs at multiple geographical locations including at the destination itself. (2) choose a long attack duration greater than the replay window duration, such that *DeLorean* does not have sufficient recorded states to replay during recovery. (3) attempt to corrupt the historic states through stealthy attacks [29], and thereby trick *DeLorean* into using the corrupted historic states for recovery.

**SDA in multiple zones:** We perform an experiment on ArduCopter, and launch SDAs targeting all the sensors at 3 different zones (1, 2, 3) during the mission. Figure 10b shows the original mission path where the RV attains an altitude of 30m, navigates towards A, then navigates towards B, and finally lands at the target.

Figure 10a shows *DeLorean*'s recovery. The first instance of SDA is launched at 30s. As can be seen, without *DeLorean* the drone crashes. In contrast, *DeLorean* replays the historic states recorded in 10-25.5s window (Table II) and recovers

the drone. This is shown in Figure 10a, in which the altitude is maintained at 30m. However, due to recovery activation, the drone missed the turn towards **B**. The course correction module detects the deviation, and calculates a new path to **B**. The second instance of SDA is launched at 120s. *DeLorean* again activates recovery, as can be seen in Figure 10a, *DeLorean* maintains the drone's altitude at 30m between  $t=120$  to  $t=140$ s. Thus, *DeLorean* successfully recovers the drone from the second SDA as well. However, while navigating towards the target the drone re-entered the attack zone which again activated recovery. After the drone exited the attack zone, a new path was calculated and the drone navigates towards the target.

The third instance of the SDA overlapped the destination. *DeLorean* recovers the drone from the third SDA as well (the altitude is maintained at 30m between 180-200s as shown in Figure 10a). When recovery is activated *DeLorean* monitors (Figure 7b) if the distance to destination in the final stretch i.e., distance from **P** to **3** is  $>$  distance traveled in the final stretch, *DeLorean* activated land mode, and the drone successfully completed the mission. However, due to recovery activation the drone covered a larger distance than planned, resulting in 1.75X increase in mission duration.

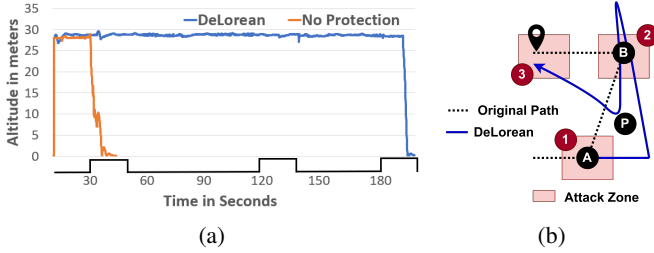


Fig. 10: *DeLorean*'s recovery in multi-zone SDA scenario. (a) with and without *DeLorean*, SDA launched 30-50s, 120-140s, 180-200s (bottom graph), (b) RV's trajectory under recovery.

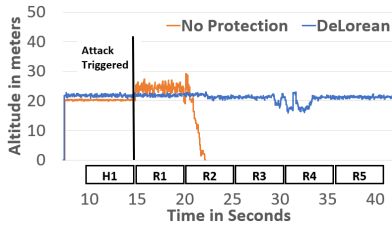


Fig. 11: *DeLorean*'s recovery for the Pixhawk drone when the attack duration  $\gg$  recording window.

**Long Duration Attack:** We mount this attack on the Pixhawk drone. Recall that when the attack range is larger than the distance covered by the recorded states, *DeLorean* iteratively replays the historic states until the RV moves out of the attack zone. In this mission, *DeLorean* records the historic states in the window H1 ( $t=10$  to 15s). At  $t=15$ s, we launch a single sensor SDA targeting the gyroscope sensor. Starting  $t=20$ s, we launch a multi-sensor SDA targeting all the sensors. Figure 11 shows *DeLorean*'s recovery under the attacks. As can be seen, without *DeLorean*, in the window R2, the drone crashes due to the SDA. However, by iteratively replaying the historical states, *DeLorean* is able to prevent the crash and recover the

drone from SDA by maintaining the altitude of the drone at 20m for the entire duration of the attack (from 15-40s). Thus, *DeLorean*'s replay-based recovery is not tied to a specific attack duration.

**Stealthy Attacks** We set a recording window large enough that a stealthy attack that injects persistent bias can be detected in one sliding window using CUSUM [30]. Thus, to deceive *DeLorean*, the attacker will need to intermittently perform stealthy attacks for a prolonged duration just to corrupt the recorded states. We assume that instead of constant bias the attacker can inject gradually increasing bias. Then, the attacker would increase the bias to cause recovery activation. Because the stealthy attack remained undetected, *DeLorean* will replay the corrupted historic states.

We perform experiments on the ArduCopter to understand the impact of the intermittently performed stealthy attack on *DeLorean*. We assume that the attacker can perform stealthy attacks that either target a single sensor or all the sensors of the RV, while avoiding detection for as long as possible. This is advantageous for the attacker because a long attack duration results in corruption in the recorded historic states. First, we performed a stealthy attack intermittently while ensuring that the attack remains undetected. This caused a total deviation of 2.1m from the drone's original path. *DeLorean* recorded the corrupted historic states as no alarm was raised by the attack detector. Then, we increased the bias, which resulted in the attack being detected, and *DeLorean* activating recovery (details in Appendix X-G). We found that *DeLorean* is able to successfully recover the drone despite the corruptions in the recorded states due to the attack. This is because the corruption in historic states due to the stealthy attack is negligible, and hence replaying them does not disrupt the RV's mission.

## VII. LIMITATIONS AND DISCUSSION

**Environmental Disturbance** *DeLorean*'s recovery suffers significantly when there are severe environmental disturbances, e.g., strong wind conditions. This is because under external disturbance, the PID controller cannot stabilize the RV simply using the historic states. Thus, on some occasions the RV overshoots the set path which results in a crash or missing the target. PID controllers can be tuned differently for strong wind conditions to allow for dynamic control. Note however that the chances of encountering such severe disturbances at the time of the attack are low, especially as the attacker cannot control the RV's environment (Section II-C).

**Continuous Signal Injection** If signal emitters are placed all along the RV's path to launch SDAs continuously, *DeLorean*'s can only prevent a crash, and will not be able to drive the RV towards the destination. However, it is challenging for the attacker to determine the RV's exact path and place signal emitters all along the path.

**Deployment Scenarios** *DeLorean* will not work in the presence of obstacles in the mission path, which is also the case for PID-Piper [30] and SSR [27]. RVs based on PID controller require a supplementary component in the feedback control loop and sensors such as camera and LiDAR to maneuver safely around obstacles. For RV's equipped with obstacle avoidance components (including camera and LiDAR), *DeLorean* can



be extended to work with obstacle avoidance systems [32] to adjust the heading direction and velocity leveraging the geometric characteristics of the RV's trajectory under recovery to maneuver the RV safely around obstacles.

**Advanced Sensors** We evaluate *DeLorean* on GPS, gyroscope, accelerometer, magnetometer, and barometer sensors that can be manipulated through physical attacks that inject fake signals. The autonomous operations in most industrial RVs today rely on the mentioned sensors [17], [19]. Recently however, RV manufacturers have started using advanced sensors such as camera and LiDAR [18]. Attacks have been demonstrated targeting both the camera and LiDAR to deceive the machine learning models (ML) that are used for image classification [25], [39]. However, these attacks are crafted for specialized ML models, and are hence out of our scope.

## VIII. RELATED WORK

Physical attacks through GPS spoofing, optical sensor spoofing, acoustic signals and magnetic signals have been demonstrated against RVs [31], [44], [45], [51], autonomous vehicles [39], [50], and smart devices [44], [54]. Many attack detection techniques have been proposed for RVs [22], [28], [30], [40], [46], [55], and other cyber physical systems (CPS) [20], [26], [34] that detect attacks based on either invariants or model estimations. However, all of these techniques focus only on attack detection, and provide neither attack diagnosis nor attack recovery, which are important for RVs.

To our knowledge, only two techniques, SSR and PID-Piper have demonstrated attack recovery in real RVs [27], [30]. We have studied these in detail earlier. Fei et al. [33] have proposed Reinforcement learning (RL) for recovering RVs from faults and attacks. Unlike *DeLorean* and similar to PID-Piper and SSR, their technique also requires a model which is trained with representative faults and attacks. Zhang et al. proposed a technique that uses reachability analysis to recover CPS from attacks [56]. There are two main differences with our work. First, they do not perform attack diagnosis. Instead, their technique considers that an attack targets all the sensors in every case, which as we have seen, is less effective than targeted diagnosis and recovery. Second, they consider a simple attack scenario where the attack is confined to a 5s window. In contrast, we consider strong attacks as well as adaptive attacks.

Recent work proposed an anti-spoofing technique that leverages IMU sensors to counteract GPS spoofing [49]. However, this method will not be effective if an SDA targets all the sensors in an RV. In contrast, *DeLorean* can recover from SDAs targeting all the sensors.

## IX. CONCLUSION

We presented *DeLorean*, a model-free framework for recovering robotic vehicles (RVs) from Sensor Deception Attacks (SDAs). *DeLorean* inspects the attack induced errors in the RV's physical states using factor graphs, and identifies the sensors targeted by SDAs. It then prevents the targeted sensors from being used to derive actuator signals, and instead replays a sequence of historic states in the RV's feedback control loop as a temporary mitigation to derive safe actuator signals. We evaluate *DeLorean* on four real and two simulated RVs.

We find that *DeLorean* (1) recovers the RVs from SDAs, and achieves mission success in 90.7% of the cases, (2) achieves mission success even against adaptive attacks, and (3) incurs modest performance, memory and battery overheads.

## REFERENCES

- [1] "Agriculture spraying drone," <https://www.dji.com/ca/t16>.
- [2] "Aimsim simple-flight," <https://microsoft.github.io/AirSim/simple-flight>.
- [3] "Aion r1 ardupilot edition," <https://docs.aionrobotics.com/en/latest/r1-ugv.html>.
- [4] "Amazon robotics," <https://robots.ieee.org/robots/kiva/>.
- [5] "ArduPilot - software in the loop," <http://ardupilot.org/dev/docs/sitl-simulator-software-in-the-loop.html>.
- [6] "Beaufort wind scale," <https://www.weather.gov/mfl/beaufort>.
- [7] "A downed drone highlights a vulnerable technology," <https://www.washingtonpost.com/politics/2023/03/16/downed-us-drone-points-cyber-vulnerabilities/>.
- [8] "Gazebo robot simulation," <http://gazebo.org/>.
- [9] Official u.s. government information about the global positioning system (gps) and related topics. [Online]. Available: <https://www.gps.gov/technical/ps/2008-SPS-performance-standard.pdf>
- [10] "Paparazzi uav," [https://wiki.paparazziuav.org/wiki/Main\\_Page](https://wiki.paparazziuav.org/wiki/Main_Page).
- [11] "Pid-piper code," <https://github.com/DependableSystemsLab/pid-piper>.
- [12] "Pixhawk autopilot," [https://docs.px4.io/en/flight\\_controller/pixhawk-series.html](https://docs.px4.io/en/flight_controller/pixhawk-series.html).
- [13] "Sky viper journey drone," <https://sky-viper.com/journey/>.
- [14] "System identification overview," <https://www.mathworks.com/help/ident/gs/about-system-identification.html>.
- [15] "Tarot 650 v2 drone," <https://uavsystemsinternational.com/products/tarot-650-ready-to-fly-drone>.
- [16] "u-blox m8 concurrent gnss modules," <https://www.u-blox.com/en/product/neo-m8-series>.
- [17] "Walmart drone delivery," <https://www.droneup.com/>.
- [18] "Wingcopter," <https://wingcopter.com/wingcopter-198>.
- [19] "Zipline drone delivery," <http://www.flyzipline.com/>.
- [20] C. M. Ahmed, J. Zhou, and A. P. Mathur, "Noise matters: Using sensor and process noise fingerprint to detect stealthy cyber attacks and authenticate sensors in cps," in *Proceedings of the 34th Annual Computer Security Applications Conference*, ser. ACSAC '18. New York, NY, USA: ACM, 2018, pp. 566–581. [Online]. Available: <http://doi.acm.org/10.1145/3274694.3274748>
- [21] D. M. Bevilacqua and B. Parkinson, "Cascaded kalman filters for accurate estimation of multiple biases, dead-reckoning navigation, and full state feedback control of ground vehicles," *IEEE Transactions on Control Systems Technology*, vol. 15, no. 2, pp. 199–208, 2007.
- [22] A. Bezemskij, G. Loukas, R. J. Anthony, and D. Gan, "Behaviour-based anomaly detection of cyber-physical attacks on a robotic vehicle," in *2016 15th International Conference on Ubiquitous Computing and Communications and 2016 International Symposium on Cyberspace and Security (IUCC-CSS)*, Dec 2016, pp. 61–68.
- [23] P. Cao, E. Badger, Z. Kalbarczyk, R. Iyer, and A. Slagell, "Preemptive intrusion detection: Theoretical framework and real-world measurements," in *Proceedings of the 2015 Symposium and Bootcamp on the Science of Security*, ser. HotSoS '15. New York, NY, USA: Association for Computing Machinery, 2015. [Online]. Available: <https://doi.org/10.1145/2746194.2746199>
- [24] Y. Cao, N. Wang, C. Xiao, D. Yang, J. Fang, R. Yang, Q. A. Chen, M. Liu, and B. Li, "Invisible for both camera and lidar: Security of multi-sensor fusion based perception in autonomous driving under physical-world attacks," *2021 IEEE Symposium on Security and Privacy (SP)*, May 2021. [Online]. Available: <http://dx.doi.org/10.1109/SP40001.2021.00076>
- [25] Y. Cao, C. Xiao, D. Yang, J. Fang, R. Yang, M. Liu, and B. Li, "Adversarial objects against lidar-based autonomous driving systems," *arXiv preprint arXiv:1907.05418*, 2019.

- [26] Y. Chen, C. M. Poskitt, and J. Sun, "Learning from mutants: Using code mutation to learn and monitor invariants of a cyber-physical system," in *2018 IEEE Symposium on Security and Privacy (SP)*. Los Alamitos, CA, USA: IEEE Computer Society, May 2018, pp. 648–660. [Online]. Available: <https://doi.ieeecomputersociety.org/10.1109/SP.2018.00016>
- [27] H. Choi, S. Kate, Y. Aafer, X. Zhang, and D. Xu, "Software-based realtime recovery from sensor attacks on robotic vehicles," in *23rd International Symposium on Research in Attacks, Intrusions and Defenses (RAID 2020)*. San Sebastian: USENIX Association, Oct. 2020, pp. 349–364.
- [28] H. Choi, W.-C. Lee, Y. Aafer, F. Fei, Z. Tu, X. Zhang, D. Xu, and X. Deng, "Detecting attacks against robotic vehicles: A control invariant approach," in *Proceedings of the 2018 ACM SIGSAC Conference on Computer and Communications Security*, ser. CCS '18. New York, NY, USA: ACM, 2018, pp. 801–816. [Online]. Available: <http://doi.acm.org/10.1145/3243734.3243752>
- [29] P. Dash, M. Karimibiuki, and K. Pattabiraman, "Out of control: Stealthy attacks against robotic vehicles protected by control-based techniques," in *Proceedings of the 35th Annual Computer Security Applications Conference*, ser. ACSAC '19. New York, NY, USA: ACM, 2019, pp. 660–672. [Online]. Available: <http://doi.acm.org/10.1145/3359789.3359847>
- [30] P. Dash, G. Li, Z. Chen, M. Karimibiuki, and K. Pattabiraman, "Pid-piper: Recovering robotic vehicles from physical attacks," in *2021 51st Annual IEEE/IFIP International Conference on Dependable Systems and Networks (DSN)*, 2021, pp. 26–38.
- [31] D. Davidson, H. Wu, R. Jellinek, V. Singh, and T. Ristenpart, "Controlling uavs with sensor input spoofing attacks," in *10th USENIX Workshop on Offensive Technologies (WOOT 16)*. Austin, TX: USENIX Association, Aug. 2016. [Online]. Available: <https://www.usenix.org/conference/woot16/workshop-program/presentation/davidson>
- [32] J. Dentler, S. Kannan, M. A. O. Mendez, and H. Voos, "A real-time model predictive position control with collision avoidance for commercial low-cost quadrotors," in *2016 IEEE Conference on Control Applications (CCA)*, 2016, pp. 519–525.
- [33] F. Fei, Z. Tu, D. Xu, and X. Deng, "Learn-to-recover: Retrofitting uavs with reinforcement learning-assisted flight control under cyber-physical attacks," in *2020 IEEE International Conference on Robotics and Automation (ICRA)*, 2020, pp. 7358–7364.
- [34] M. Gauthama Raman, W. Dong, and A. Mathur, "Deep autoencoders as anomaly detectors: Method and case study in a distributed water treatment plant," *Computers and Security*, vol. 99, p. 102055, 2020. [Online]. Available: <https://www.sciencedirect.com/science/article/pii/S016740482030328X>
- [35] D. Hambling, "Uk ship hit by gps spoof," *New Scientist*, vol. 250, no. 3341, p. 17, 2021. [Online]. Available: <https://www.sciencedirect.com/science/article/pii/S0262407921011313>
- [36] K. Hartmann and C. Steup, "The vulnerability of uavs to cyber attacks—an approach to the risk assessment," in *2013 5th international conference on cyber conflict (CYCON 2013)*. IEEE, 2013, pp. 1–23.
- [37] A. J. Hawkins, "Ups will use drones to deliver medical supplies in north carolina." [Online]. Available: <https://www.theverge.com/2019/3/26/18282291/ups-drone-delivery-hospital-nc-maternet>
- [38] T. E. Humphreys, "Assessing the spoofing threat: Development of a portable gps civilian spoofer," in *In Proceedings of the Institute of Navigation GNSS (ION GNSS)*, 2008.
- [39] X. Ji, Y. Cheng, Y. Zhang, K. Wang, C. Yan, W. Xu, and K. Fu, "Poltergeist: Acoustic adversarial machine learning against cameras and computer vision," in *2021 IEEE Symposium on Security and Privacy (SP)*. IEEE, 2021, pp. 160–175.
- [40] A. Khan, H. Kim, B. Lee, D. Xu, A. Bianchi, and D. J. Tian, "M2mon: Building an mmio-based security reference monitor for unmanned vehicles," in *30th {USENIX} Security Symposium ({USENIX} Security 21)*, 2021.
- [41] J. Li and Y. Li, "Dynamic analysis and pid control for a quadrotor," in *2011 IEEE International Conference on Mechatronics and Automation*, Aug 2011, pp. 573–578.
- [42] Y. Lin and S. Saripalli, "Sense and avoid for unmanned aerial vehicles using ads-b," in *2015 IEEE International Conference on Robotics and Automation (ICRA)*. IEEE, 2015, pp. 6402–6407.
- [43] L. Meier, P. Tanskanen, F. Fraundorfer, and M. Pollefeys, "Pixhawk: A system for autonomous flight using onboard computer vision," in *2011 IEEE International Conference on Robotics and Automation*. IEEE, 2011, pp. 2992–2997.
- [44] S. Nashimoto, D. Suzuki, T. Sugawara, and K. Sakiyama, "Sensor con-fusion: Defeating kalman filter in signal injection attack," in *Proceedings of the 2018 on Asia Conference on Computer and Communications Security*, ser. ASIACCS '18. New York, NY, USA: Association for Computing Machinery, 2018, p. 511–524. [Online]. Available: <https://doi.org/10.1145/3196494.3196506>
- [45] J. Noh, Y. Kwon, Y. Son, H. Shin, D. Kim, J. Choi, and Y. Kim, "Tractor beam: Safe-hijacking of consumer drones with adaptive gps spoofing," *ACM Transactions on Privacy and Security (TOPS)*, vol. 22, no. 2, pp. 1–26, 2019.
- [46] R. Quinonez, J. Giraldo, L. Salazar, E. Bauman, A. Cardenas, and Z. Lin, "SAVIOR: Securing autonomous vehicles with robust physical invariants," in *29th USENIX Security Symposium (USENIX Security 20)*. Boston, MA: USENIX Association, Aug. 2020.
- [47] C. Reimann, P. Filzmoser, and R. G. Garrett, "Background and threshold: critical comparison of methods of determination," *Science of The Total Environment*, vol. 346, no. 1, pp. 1–16, 2005. [Online]. Available: <https://www.sciencedirect.com/science/article/pii/S0048969704007983>
- [48] B. A. Renfro, M. Stein, N. Boeker, E. Reed, and E. Villalba, "An analysis of global positioning system (gps) standard positioning service (sp) performance for 2018," editor, Ed.
- [49] H. Sathaye, G. LaMountain, P. Closas, and A. Ranganathan, "Semperfi: Anti-spoofing gps receiver for uavs," in *Network and Distributed Systems Security (NDSS) Symposium 2022*, 2022.
- [50] Y. Shoukry, P. Martin, P. Tabuada, and M. Srivastava, "Non-invasive spoofing attacks for anti-lock braking systems," in *Cryptographic Hardware and Embedded Systems - CHES 2013*, G. Bertoni and J.-S. Coron, Eds. Berlin, Heidelberg: Springer Berlin Heidelberg, 2013, pp. 55–72.
- [51] Y. Son, H. Shin, D. Kim, Y. Park, J. Noh, K. Choi, J. Choi, and Y. Kim, "Rocking drones with intentional sound noise on gyroscopic sensors," in *24th USENIX Security Symposium (USENIX Security 15)*. Washington, D.C.: USENIX Association, 2015, pp. 881–896. [Online]. Available: <https://www.usenix.org/conference/usenixsecurity15/technical-sessions/presentation/son>
- [52] N. O. Tippenhauer, C. Pöpper, K. B. Rasmussen, and S. Capkun, "On the requirements for successful gps spoofing attacks," in *Proceedings of the 18th ACM Conference on Computer and Communications Security*, ser. CCS '11. New York, NY, USA: ACM, 2011, pp. 75–86. [Online]. Available: <http://doi.acm.org/10.1145/2046707.2046719>
- [53] T. Trippel, O. Weisse, W. Xu, P. Honeyman, and K. Fu, "Walnut: Waging doubt on the integrity of mems accelerometers with acoustic injection attacks," in *2017 IEEE European Symposium on Security and Privacy (EuroS P)*, April 2017, pp. 3–18.
- [54] Y. Tu, Z. Lin, I. Lee, and X. Hei, "Injected and delivered: Fabricating implicit control over actuation systems by spoofing inertial sensors," in *27th USENIX Security Symposium (USENIX Security 18)*. Baltimore, MD: USENIX Association, Aug. 2018, pp. 1545–1562. [Online]. Available: <https://www.usenix.org/conference/usenixsecurity18/presentation/tu>
- [55] N. Xue, L. Niu, X. Hong, Z. Li, L. Hoffaeller, and C. Pöpper, "Deepsim: Gps spoofing detection on uavs using satellite imagery matching," in *Annual Computer Security Applications Conference*, ser. ACSAC '20. New York, NY, USA: Association for Computing Machinery, 2020, p. 304–319. [Online]. Available: <https://doi.org/10.1145/3427228.3427254>
- [56] L. Zhang, P. Lu, F. Kong, X. Chen, O. Sokolsky, and I. Lee, "Real-time attack-recovery for cyber-physical systems using linear-quadratic regulator," *ACM Trans. Embed. Comput. Syst.*, vol. 20, no. 5s, Sep 2021. [Online]. Available: <https://doi.org/10.1145/3477010>

## APPENDIX

### X. APPENDIX

#### A. Erroneous Physical States due to SDA

Figure 12 shows the attack induced error in RV's physical states for the experiment discussed in Section III. For

TABLE VIII:  $\delta$  values for per sensor factor graphs in each subject RVs. position  $(x, y, z)$  in meters (m), velocity  $(\dot{x}, \dot{y}, \dot{z})$  in  $m/s$ , acceleration  $(\ddot{x}, \ddot{y}, \ddot{z})$  in  $m/s^2$ , Euler angles  $(\phi, \theta, \psi)$  in degrees, angular velocities  $(\omega_\phi, \omega_\theta, \omega_\psi)$  in rad/s, magnetic fields  $(x_m, y_m, z_m)$  in Gauss(G), Altitude in m. (values are rounded up to 1st decimal place)

RV Type	GPS						Accel			Gyroscope						Mag			Baro	Window Size
	$x$	$y$	$z$	$\dot{x}$	$\dot{y}$	$\dot{z}$	$\ddot{x}$	$\ddot{y}$	$\ddot{z}$	$\phi$	$\theta$	$\psi$	$\dot{\phi}$	$\dot{\theta}$	$\dot{\psi}$	$x_m$	$y_m$	$z_m$	Alt	
Pixhawk	3.4	5.1	5.2	2.1	10.2	5.5	6.5	4.2	10.5	12.2	9.8	45.5	11.5	13.8	1.1	0.6	0.3	0.5	0.2	15.5s
Tarrot	5.5	3.4	6.5	1.8	8.1	4.2	8.1	7.7	9.2	10.2	9.5	38.9	10.2	10.6	1.1	0.3	0.3	0.4	0.2	15s
Sky-Viper	4.6	3.0	4.1	1.7	7.8	3.1	5.5	4.2	5.6	13.3	11.2	58.5	14.5	16.1	1.5	0.6	0.6	0.5	0.2	17s
AionR1	2.7	2.5	-	1.9	6.4	-	3.3	3.5	-	-	-	45.2	-	-	2.2	-	-	-	-	18.5s
ArduCopter	3.7	3.3	4.5	2.1	9.3	4.2	5.2	6.5	7.1	9.7	9.5	36.2	9.5	11.2	1.1	0.3	0.2	0.5	0.1	15.5s
ArduRover	4.2	4.1	-	2.4	7.3	-	3.5	3.9	-	-	-	38.5	-	-	1.8	-	-	-	-	17s

simplicity, we show 2 out of 15 physical states of the RV. Figure 12a and Figure 12b shows the change of roll angle and pitch angles respectively under SDA. Note that as the drone is navigating in a straight line at a fixed altitude, the roll angle should be 0, because the drone is not rotating along its  $x$  axis. Similarly, after takeoff, the drone's pitch angle should be -30 approximately when navigating in a straight line. As we can see in Figure 12a, during the attack free phase of the mission (0-10s), the roll angle is 0 degrees. The attack starts after 10s, and as a result, the roll rate fluctuates between -30 and +30 degrees (Figure 12a). Similar trends can be seen for pitch angle (Figure 12b), just before the attack started the pitch angle was set at -30 degrees and should remain constant for the entire duration of the mission. Under attack, the pitch angle fluctuates between -35 and +12 degrees. Thus, attack induced sensor manipulations result in erroneous physical states.

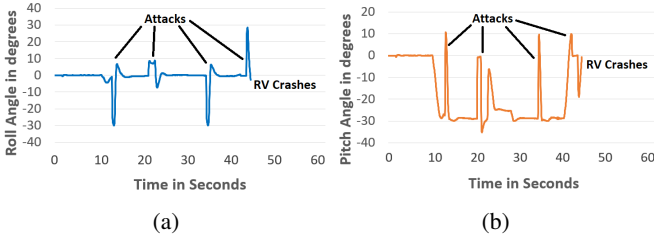


Fig. 12: (a) Roll angle fluctuations, (b) Pitch angle fluctuations of Pixhawk drone due to SDA targeting all the sensors simultaneously.

In Section III, Figure 2a showed the error inflation between target and observed roll and pitch angles, and how the error inflation results in the PID controller issuing erroneous actuator signals.

### B. Controlled State Estimation Error under Recovery

In this section, we show how robust actuator signals are derived to recover the RV from SDA by replaying historic physical states in the RV's feedback control loop.

Figure 13a and Figure 13b shows the error in the target and the current physical state ( $e_s = \text{target} - \text{current}$ ) of the Sky-viper drone under recovery. An SDA targeting all the sensors was launched from  $t=25$  to  $45s$ . Recall that without *DeLorean* the error  $e_s$  fluctuates due to the SDA (Section III). In contrast, with *DeLorean* the error in RV's physical states are controlled (non-fluctuating). As can be seen in Figure 13a, under recovery, the error in RV's roll and pitch angles remain

between -0.25 and +0.25 degrees. Similarly, in Figure 13b, the RV's X and Y position error in non-fluctuating, it increases and decreases in a steady manner. As the corruptions in the PID controller's input are controlled, the actuator signals derived by the PID controller do not fluctuate which safely maneuvers the RV. Figure 13c shows the output of motor-1 as an example which is set at 0.65 under recovery (from  $t=25s$  to  $t=45s$ ).

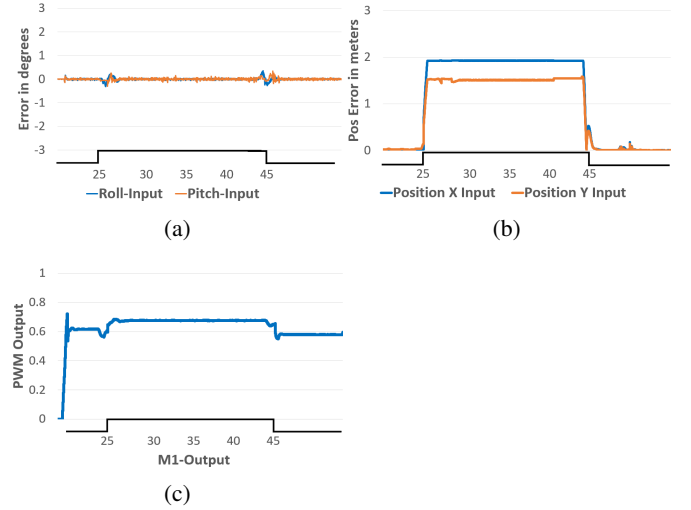


Fig. 13: (a) Roll and Pitch angle under recovery. (b) Position X and Y under recovery. (c) Actuator signal under recovery of Pixhawk drone.

### C. Joint Probability and Factor Graphs

The joint probability of variables  $x_1, \dots, x_n$  is described as  $P(x_1, \dots, x_n)$ . Causal inference of an event given the observed variable is calculated as:  $y = \text{argmax}_y P(y|x_1, \dots, x_{n-1})$ , which can be further expanded as the following.

$$P(y|x_1, \dots, x_{n-1}) = \frac{P(x_1, \dots, x_{n-1})}{\sum_v P(x_1, \dots, x_{n-1}, y = v)} \quad (6)$$

Inference on a joint probability distribution  $P(x_1, \dots, x_n)$  requires  $2^n$  storage for events with binary outcome (e.g., malicious, benign), which is computationally expensive as well.

Factor graphs can be used to overcome this problem. A factor graph (FG) is probabilistic graphical model that allows expressing joint probability as product of smaller local functions [23]. Figure 14 shows an example. There are two

types of nodes in a FG namely variables ( $x_1, x_2, x_3$ ) and factor functions ( $f_1, f_2, f_3$ ). Variables are used to quantitatively describe an event. A factor function is used to express relationship among variables.

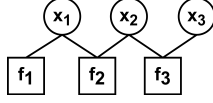


Fig. 14: An example of factor graph

Let's take Figure 14 as an example to understand how to calculate conditional probability using factor graph. The variables  $x_1, x_2, x_3 \in X$ , and  $y$  is the outcome.  $P(x_1, x_2, x_3)$  can be factored as a product of  $f_1, f_2, f_3$ .

$$P(x_1, x_2, x_3) = f_1(x_1), f_2(x_1, x_2), f_3(x_2, x_3) \quad (7)$$

Thus, conditional probability of an event given the observed variables is calculated as:

$$P(y|x_1, x_2, x_3) = \prod_{f \in F} f(x) \quad (8)$$

Using sum product algorithm, the marginal is defined as  $P(x) = \sum_{x \in X} P(X)$ . Thus, the conditional probability of an event given the observed variables is calculated as the following.

$$P(y|x_1, x_2, x_3) = \sum f(x) \quad (9)$$

#### D. Diagnosis parameters

Figure 15 shows an example of  $\delta$  for position error and pitch angle in the Pixhawk drone. The figure shows the Cumulative Distribution Function (CDF) of error  $e$  as a function of the probability that the physical states errors will take a value less than  $\delta$ . With  $k = 3$ , we obtain the  $\delta$  values for  $z$ -axis position error as 5.2 and 9.81 for pitch angle error. As shown in Figure 15, in the attack-free phase, the error  $e$  always remains under the  $\delta$  value. We derive  $\delta$  for all the physical states of the RV in the same manner, shown in Table VIII.

To calculate the above values, for each simulated RV, we run 60 missions, each of which lasts for 120s (on average). For the real RV, we run between 15-25 missions across RVs, lasting 50-90s each. Therefore, the total effort for calculating  $\delta$  is about 120 minutes for each simulated RV, and about 28 minutes for each real RV. This is a one time cost for each RV.

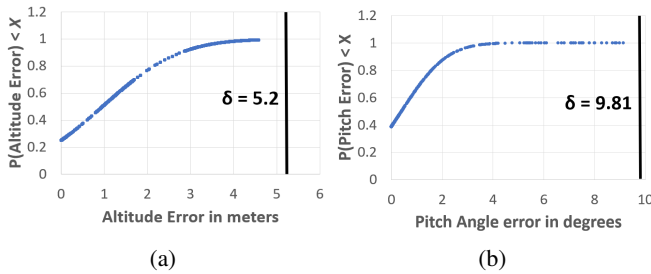


Fig. 15: CDF of error distribution in the Pixhawk drone.  $k = 3$  ensures  $0 < e < \delta$  in attack-free phase.

#### E. Course Correction

The course correction algorithm uses the Dijkstra's shortest path algorithm to find the shortest path to the destination from the position of the RV after it has left the attack zone. Figure 16 shows the course correction procedure. The main steps are as follows: i) At the start of the mission, we calculate the distance  $D_w$  to the waypoint as per the defined trajectory. ii) We keep track of the distance traveled  $d_t$  as the mission progresses, and the distance left to cover as  $d_g$  ( $d_g = D_w - d_t$ ). iii) When recovery is activated, we stop updating  $d_t$ , and we keep track of the distance traveled under the attack  $d_a$ . iv) When the RV is out of the attack zone (based on the attack detector's response), we recalculate  $d_g$  and check if  $D_w > d_t + d_a + d_g$ . If the condition is true, it means the RV has veered from its trajectory, and hence we recalculate the path.

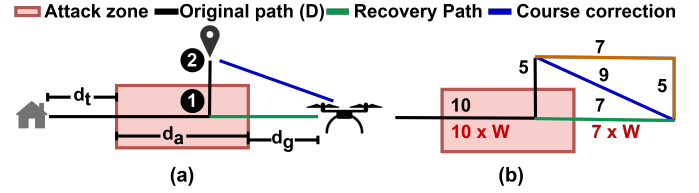


Fig. 16: (a) Course correction after the RV is out of the attack zone. (b) *DeLorean* finds the shortest path for course correction after leaving the attack zone.

However, there is one corner case where it is possible that the shortest path to the destination derived using Dijkstra's algorithm takes the RV back to the attack zone, which is not desirable. We prevent the RV from going back to the attack zone by increasing the weights of the paths through the attack zone, which makes them much more expensive. Hence, they will be avoided by the shortest path algorithm (as shown in Figure 16b).

Algorithm 2 shows the steps for course correction. Once the attack subsides based on attack detector's response, *DeLorean* checks if the RV has veered off its trajectory (Line 10). If so, *DeLorean* activates course correction and calculates a new path to the next waypoint (Line 11-12). The RV's navigation module is updated as per the new path (Line 13). To avoid the RV from going back into the attack zone, the weight of the path being recovered from is increased (Line 14). To handle case where the RV's destination is in the attack zone, we add a check in the course correction algorithm to check if the total distance traveled without recovery ( $d_t$ ) and with recovery ( $d_a$ ) is  $\geq$  distance to destination ( $d_g$ ), if so, we signal to complete the mission.

#### F. Mission Types

We run a diverse set of missions to derive the experimental parameters and for our experiments. Table IX shows the details.

#### G. Recovery Under Stealthy Attacks

We performed a stealthy attack intermittently from 10-20s while ensuring that the stealthy attack remains undetected. This caused a total deviation of 2.1m from the drone's original path (Figure 17a). *DeLorean* recorded the corrupted historic states



---

**Algorithm 2** Algorithm for Course Correction
 

---

```

1:  $D \leftarrow$  distance to destination
2:  $D_w \leftarrow$  distance to waypoint  $w$ 
3:  $d_t \leftarrow$  distance traveled
4:  $d_g \leftarrow$  distance to cover
5:  $d_a \leftarrow$  distance traveled under attack
6:  $p_i \leftarrow$  original mission path
7:  $p_a \leftarrow$  path under recovery
8:  $p_r \leftarrow$  path during course correction
9: procedure COURSE CORRECTION
10:   if !alert and recovery_mode  $\leftarrow$  true then
11:     if  $D_w > d_t + d_g + d_a$  then
12:        $source \leftarrow GPS()$  ▷ current Location
13:        $p_r \leftarrow shortest\_path(source, destination)$ 
14:        $update\_nav(p_r)$  ▷ update mission trajectory
15:        $p_a \leftarrow w * x$  ▷ update weight of  $p_a$ 
16:     end if
17:   else
18:      $d_a \leftarrow update\ d_a$ 
19:     if  $D > d_t + d_a$  then
20:        $command \leftarrow$  complete mission
21:     end if
22:   end if
23: end procedure
  
```

---

TABLE IX: Mission paths used in evaluating *DeLorean*. S: Straight line, MW: Multiple waypoints, C: Circular, and Three different polygonal paths P1, P2, and P3

Mission Paths	S	MW	C	P1	P2	P3	Total
Number of missions	70	70	50	50	50	50	340

as no alarm was raised by the attack detector. From 25-45s we launched an SDA, which is detected instantly, and *DeLorean* activates recovery (Figure 17b). As can be seen, *DeLorean* is able to recover the drone and maintain the altitude at 20m despite the corruptions in the recorded states due to the attack.

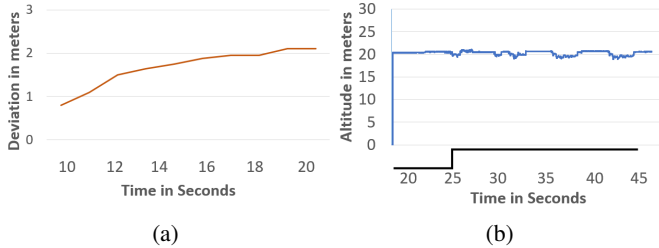


Fig. 17: *DeLorean* recovery in ArduCopter under stealthy attacks. (a) Corruptions in recorded states due to stealthy attacks, (b) Recovery under SDA targeting all the sensors.

### H. Recovery under Environmental Disturbance

Figure 18a shows *DeLorean*'s successful recovery with and without wind. Here the drone encountered strong wind after the attack was launched (scenario A). An SDA targeting all the sensors was launched from  $t=20$  to 40s. As can be seen, without wind *DeLorean* successfully recovers the drone maintaining its altitude at 10m. However, under wind, *DeLorean* struggled to maintain the drone's altitude at 10m using the historic states that do not represent the correct actions

required under windy conditions, but eventually recovers the drone from the attack.

On the other hand, in scenario B the drone encountered strong wind throughout the mission. Figure 18b shows *DeLorean*'s recovery with and without wind conditions considered in scenario B. An SDA targeting all the sensors was launched from  $t=20$  to 40s. As can be seen, *DeLorean* successfully recovered the drone both with and without wind (drone did not crash from  $t=20$ -40). However, under wind, *DeLorean* had to use noisy historic states as the wind flow started before the attack, and hence *DeLorean* failed to maintain stable 10m altitude under attack.

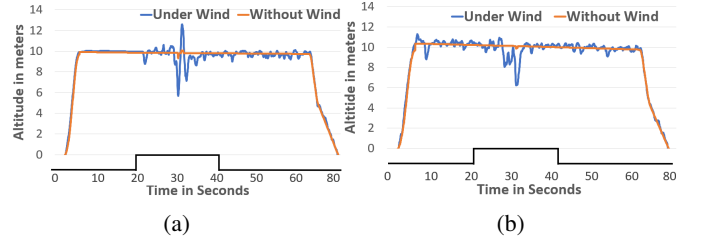


Fig. 18: *DeLorean* under environmental disturbance (wind speed 8-10 m/s), SDA targeting all the sensors launched from  $t=20$  to 40s. (a) Scenario A, (b) Scenario B.